Water Research 142 (2018) 65–74

Contents lists available at ScienceDirect

Water Research

journal homepage: www.elsevier.com/locate/watres

Hybrid algal photosynthesis and ion exchange (HAPIX) process for high ammonium strength wastewater treatment

Meng Wang [a], Karl A. Payne [a], Shuang Tong [a, b, c], Sarina J. Ergas [a, *]

[a] Department of Civil and Environmental Engineering, University of South Florida, Tampa, USA
[b] School of Water Resources and Environment, China University of Geoscience, Beijing, China
[c] Beijing Key Laboratory of Meat Processing Technology, China Meat Research Center, Beijing, China

ARTICLE INFO

Article history:
Received 19 February 2018
Received in revised form
17 May 2018
Accepted 24 May 2018
Available online 25 May 2018

Keywords:
Ion exchange
Algal photosynthesis
High ammonium strength wastewater
Mathematical modeling
Intracellular contents of algae

ABSTRACT

A hybrid algal photosynthesis and ion exchange (HAPIX) process was developed that uses natural zeolite (chabazite) and wild type algae to treat high ammonium (NH_4^+) strength wastewater. In the HAPIX process, NH_4^+ is temporarily adsorbed from the liquid, which reduces the free ammonia (FA) concentration below the inhibitory level for algal growth. The slow release of adsorbed NH_4^+ subsequently supports the continuous growth of algae. In this study, a HAPIX reactor reduced NH_4^+-N concentrations in centrate from an anaerobic digester from 1180 mg L^{-1} to below 10 mg L^{-1} without dilution. Chabazite doses of 60 g L^{-1} produced more algal biomass, with higher protein and starch contents, than doses of 150 g L^{-1} and 250 g L^{-1}. Approximately 67–70% of fatty acids in the algal biomass harvested from HAPIX reactors were unsaturated. A mathematical framework that couples a homogeneous surface diffusion model with a co-limitation algal kinetic growth model reasonably predicted the algal biomass production and NH_4^+-N concentrations in the HAPIX reactors. The HAPIX process has the potential to serve a two-fold purpose of high NH_4^+-N strength wastewater treatment and agricultural or commercial biopolymer production.

1. Introduction

Management of the nitrogen (N) cycle was identified by the National Academy of Engineering as one of the grand challenges of the 21st century. A major source of N is high ammonium (NH_4^+) strength wastewaters, such as industrial wastewaters (e.g. food processing, fertilizer, plastic industries), landfill leachate, source separated urine and centrate from anaerobic digestion. These wastewater streams are challenging and expensive to treat (Kjeldsen et al., 2002; Udert et al., 2003). Anaerobic digestion centrate is of particular interest since anaerobic digestion technology is being promoted for stabilization and bioenergy recovery from waste resources, such as sewage sludge and food waste (Cantrell et al., 2008). The high NH_4^+ strength centrate is often recycled back to the head of the wastewater treatment plant, resulting in high irregular nutrient loads that can upset mainstream biological N removal (BNR) processes and increase costs (Fux et al., 2006; Wett and Alex, 2003).

Although a number of advanced BNR processes, such as shortcut N removal (nitritation-denitritation) and anaerobic ammonium oxidation (anammox), have been developed to reduce the energy and chemical costs of high NH_4^+ strength wastewater treatment (Kotay et al., 2013; Lackner et al., 2014; Third et al., 2005), utilization of algae for treatment of these wastewater presents an opportunity for co-production of biofuels, high value chemicals and animal feeds (Li et al., 2011; Park et al., 2010; Rusten and Sahu, 2011; Wang and Park, 2015; Wang et al., 2015). The high nutrient concentrations in these wastewaters also have the potential to support higher algal biomass densities than low-strength wastewaters (e.g. secondary & tertiary effluent), resulting in lower downstream costs for thickening and dewatering (Halfhide et al., 2014). However, NH_4^+-N concentrations greater than 200–300 mg L^{-1} are known to inhibit algae growth due to the uncoupling effect of free ammonia (FA) on the photosynthetic processes in chloroplasts (Crofts, 1966; Lin et al., 2007; Park et al., 2010). Prior studies have addressed this issue by dilution with fresh water or low-strength wastewater or using a fed-batch bioreactor approach (Wang et al. 2010, 2015; Yuan et al., 2012).

* Corresponding author. 4202 E. Fowler Avenue, ENB 118, Tampa, FL 33620-5350, USA.
E-mail address: sergas@usf.edu (S.J. Ergas).

https://doi.org/10.1016/j.watres.2018.05.043
0043-1354/

Strategies to reduce the FA toxicity are needed to promote the implementation of algae cultivation in high NH_4^+ strength wastewater.

Zeolites are natural hydrated aluminosilicate materials with a high affinity for NH_4^+ ions (Malovanyy et al., 2013; Rožić et al., 2000). Compared with the polymeric cation exchange resins, natural zeolites have a lower cost per gram of N removed. In addition, shrinking and swelling in polymeric resins can occur depending on the extent of polymer cross-linking. These changes are insignificant for natural zeolites and are less likely to have an impact, which is an important consideration since some extracellular polymeric substance can deposit on the surface of the IX media (Tarpeh et al., 2017). Common forms of natural zeolite include clinoptilolite, mordenite, phillipsite, chabazite, stilbite, analcime and laumontite (Wang and Peng, 2010). Clinoptilolite is the most abundant and lowest cost natural zeolite material; however, its NH_4^+ capacity is low compared with chabazite (Amini et al., 2017; Aponte-Morales, 2015). Prior studies of biological treatment of high NH_4^+ strength wastewaters have successfully used the ion exchange (IX) capacity of natural zeolites to reduce the toxicity of FA to nitrifying prokaryotes (Aponte-Morales et al. 2016, 2018; Martins et al., 2017; Tada et al., 2005). Biological processes, such as nitrification, will consume NH_4^+ in the aqueous phase and promote desorption of NH_4^+ from the solid phase. The zeolite can therefore be biologically regenerated, thus less chemicals are required to regenerate the spent-zeolite. Prior research showed that a chabazite-amended sequencing batch reactor was able to treat anaerobically digested swine waste without loss of IX efficiency for over 40 cycles of operation (Aponte-Morales et al., 2016). Combining the IX process with algae cultivation has the potential to treat high NH_4^+ strength wastewater without dilution. The adsorbed NH_4^+ in the solid phase will be desorbed to support continuous algal growth when the NH_4^+ in the aqueous-phase is consumed. In addition, no prior studies have presented a mathematical description of IX combined with algal photosynthesis. Such a study can improve the understanding of the underlying physical, chemical and biological mechanisms.

Several prior studies have focused on surface diffusion models of IX in zeolites and microporous materials (Auerbach et al., 2003; Krishna and Wesselingh, 1997; Lito et al., 2014) or algal photosynthesis kinetics (Juneja et al., 2013; Lee and Zhang, 2016). However, coupling IX and algal photosynthesis kinetics into a mathematical framework has not previously been investigated. A prior study in our research group demonstrated that a Fickian-based continuum-scale model, the homogenous surface diffusion model (HSDM), combined with a kinetic model of FA inhibited nitrification, the Andrew's model, described IX-assisted nitrification and bioregeneration (Aponte-Morales et al., 2018). However, microalgae growth is influenced by different factors than nitrification including temperature, light availability, pH and the concentrations of nutrients such as N and phosphorus (P) (Juneja et al., 2013). A comprehensive review of the various models of microalgae growth kinetics is presented elsewhere (Lee and Zhang, 2016); in general, models of microalgae growth kinetics can be categorized as single limitation or co-limitation approaches. In single limitation models, it is commonly assumed that algal growth kinetics is either limited by a single substrate (N, P, CO_2) or light intensity. For co-limitation models, either a threshold or multiplicative conceptualization is adopted (Lee and Zhang, 2016).

In this study, we propose a novel hybrid algal photosynthesis and ion exchange (HAPIX) process to recover nutrients from high NH_4^+ strength wastewater. It is hypothesized that NH_4^+ in the wastewater will be absorbed by the zeolite and exchanged with cations such as Na^+ and K^+. Adsorption of NH_4^+ will reduce FA concentrations in the liquid phase to below inhibitory levels for algae growth. Moreover, algae grown under N-depleted conditions tend to accumulate lipids, while algae grown in high N wastewater tend to have a higher protein content (Shifrin and Chisholm, 1981; Solovchenko et al., 2008). We hypothesize that by controlling the zeolite dosages the aqueous phase NH_4^+ concentrations are regulated, which will tune the intracellular contents of harvested algae. For example, low IX doses will result in algae with a high protein content, which can be used as a biofertilizer, while high IX doses will produce algae with a high lipid content, which can be used for biofuel production.

To the best of our knowledge, this is the first study to combine IX with algal photosynthesis for high NH_4^+ strength wastewater treatment. Benefits of the HAPIX process are to: 1) reduce the toxicity of high strength NH_4^+ wastewater on microalgae; 2) handle the shock load by the hybrid IX process and enhance system stability (Jorgensen and Weatherley, 2003); 3) regulate the production of intracellular products by varying zeolite dosages. The specific objectives of this study are to: 1) evaluate the impact of zeolite dosage on the NH_4^+ removal efficiencies; 2) assess the impact of zeolite dosages on intracellular compounds of harvested algal biomass; 3) develop a mathematical model to predict NH_4^+ removal and algal biomass growth in the HAPIX reactor.

2. Materials and methods

2.1. Characteristics of anaerobic digester centrate

Centrate used in this study was obtained from a pilot anaerobic digester treating waste activated sludge from an enhanced biological N and P removal treatment facility (Tampa, Florida). The anaerobic digester had a working volume of 24 L and was operated for over 100 days under thermophilic (45–55 °C) conditions with a solids residence time (SRT) of 20 days. Effluent from the digester was centrifuged at 4000 rpm for 15 min. The supernatant from this initial solid-liquid separation step was further filtered through 1.5 μm filter paper (934-AH, Whatman). Characteristics of the centrate are summarized in Table 1.

2.2. HAPIX reactor setup

Wild-type algae, *Chlorella* (95% of the total cells), originally harvested from a local wastewater treatment plant were enriched in diluted anaerobic digester centrate for this study (Halfhide et al., 2014). Algae were settled for 24 h, and the settled algae were collected as the inoculum for the HAPIX reactors. The chlorophyll *a* and dry weight of the algal inoculum was 81.1 ± 2.5 mg L^{-1} and 5412 ± 159 mg L^{-1}, respectively. The algal inoculum was washed three times with DI water to remove residuals from the diluted sludge centrate before seeding the HAPIX reactors.

Bowie chabazite (a type of zeolite, product code: AZLB-Ca) from St. Cloud Mine (New Mexico) was sieved to obtain a particle size between 1.0 and 1.4 mm. Chabazite particles were washed with DI five times to remove fine particles. Washed chabazite was placed in 500 mL Erlenmeyer flasks with DI water and shaken at 110 rpm for 24 h. The pretreated chabazite was dried at 100 °C in an oven for the

Table 1
Characteristics of centrate from anaerobic digestion of waste activated sludge.

Parameters	Unit	Value
NH_4^+-N	mg L^{-1}	1180
PO_4^{3-}-P	mg L^{-1}	267 ± 0.0
VFA	mg L^{-1}	822 ± 4.9
COD	mg L^{-1}	2340 ± 0
Alkalinity	mg L^{-1} as $CaCO_3$	2585 ± 304
pH	–	8.0 ± 0.1

following experiments. Chabazite dosages evaluated were 60 (IA-60), 150 (IA-150) and 250 (IA-250) g L^{-1}, based on isotherm and kinetics studies (S1). The operational strategy of the HAPIX reactors is shown in Fig. 1. Briefly, 1 L Erlenmeyer flasks were set up with 500 mL of centrate and various chabazite dosages. Reactors were set up in duplicate in a 21 ± 2 °C constant temperature room. A shaking table set at 100 ± 10 rpm provided mixing for all the reactors. After 24 h' adsorption when the NH_4^+ concentration was reduced below 200 mg L^{-1}, 40 mL of pre-washed algae inoculum was added to each flask, which was recorded as Day 0 of the HAPIX process. DI water was added as needed to account for water evaporation. The reactors were continuously illuminated at 121 ± 6 μmol m^{-2} s^{-1} by three 35 W Commercial Electric white LED lights. Chabazite always remained resident at the bottom of reactors due to its high density. The HAPIX reactors were operated in three phases (Fig. 1). During Phase 1, algae were grown in the centrate after IX. Suspended algae were harvested by centrifugation at 3800 rpm for 10 min when the algal biomass concentrations reached stationary state. Supernatant after algae harvesting was replaced into the original reactors for the continuous growth of algae during Phase 2 and Phase 3. Reactors with only algal biomass were also set up as controls (A-control). Chabazite at the same dosages as HAPIX reactors without the addition of algae were set up as the IX controls (IX-60, IX-150 and IX-250). The IX controls were covered with parafilm and aluminum foil to reduce the potential biological activity.

2.3. Analytical methods

Algal biomass dry weight (total suspended solids [TSS]), total volatile solids (VSS) and alkalinity were measured according to *Standard Methods* (APHA et al., 2012). COD was measured according to *Standard Methods* (5200B) using Orbeco-Hellige mid-range (0–1500 mg L^{-1}) COD kits. Total P was measured using Hach TNT plus 845 test kits. Total N was measured by Hach TNT plus 827 and TNT 828 test kits. Volatile fatty acid (VFA) concentrations as acetic acid were measured by the esterification method using Hach TNT plus 872 test kits. Cations, including NH_4^+, Na^+, K^+, Ca^{2+}, and Mg^{2+} concentrations were measured using a Metrohm Peak 850 Professional AnCat ion chromatography (IC) system (Metrohm Inc., Switzerland).

The harvested algae were freeze-dried (Labconco, US) for starch, lipid, and protein analysis. The total starch content of the algal biomass were measured using Megazyme total starch (AA/AMG) kits (catalog # K-TSTA), following the Association of Official Agricultural Chemists (AOAC) Method 996.11. Protein content was analyzed by the bicinchionic acid colorimetric method (BAC) using Micro BC Assay Kits (Interchim, France). The lipid contents were analysis by a commercial laboratory (Eurofins Scientific, US) according to the AOAC Method 996.06.

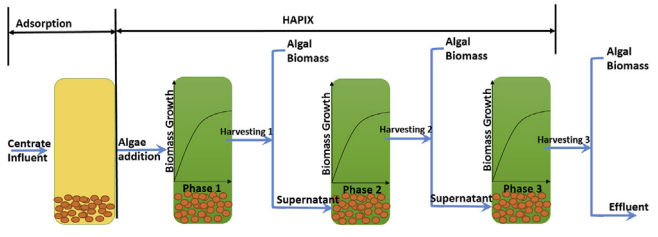

Fig. 1. Overall operational strategy of HAPIX reactors.

2.4. Statistical analysis

The statistical differences of the nitrogen removal and intracellular contents of algae at different zeolite dosages were evaluated by ANOVA ($P < 0.05$) using Excel 2013 (Microsoft, US).

3. Mathematical modeling

A mathematical model was developed to test the hypothesis that IX and photosynthetic growth of algae captures the processes of NH_4^+ removal and algal biomass production in the HAPIX reactors. The model considers the limiting diffusion process as intraparticle surface diffusion, which is characterized by probabilistically rare hops of ions between IX sites in the zeolite framework (Auerbach et al., 2003). For ionic fluxes based on Fickian diffusion, the flux term is given by:

$$J_{NH_4^+} = -\rho D_s \left.\frac{\partial q_{NH_4^+}}{\partial r}\right|_{r=R} \quad (1)$$

where $J_{NH_4^+}$ (meq m^{-2} h^{-1}) is the flux of NH_4^+ ions, ρ (g m^{-3}) is the density of the chabazite particles, D_s (m^2 h^{-1}) is the surface diffusivity, r (m) is the radial coordinate within the solid material, $q_{NH_4^+}$ (meq g^{-1}) is the solid-phase NH_4^+ concentration, and R (m) is the radius of a chabazite particle. In the solid phase, the mass balance is given by:

$$\frac{\partial q_{NH_4^+}}{\partial t} = \frac{D_s}{r^2}\frac{\partial}{\partial r}\left(r^2 \frac{\partial q_{NH_4^+}}{\partial r}\right) \quad (2)$$

where r (m) is the radial coordinate within the solid material, $q_{NH_4^+}$ (meq g^{-1}) is the solid-phase NH_4^+ concentration (meq g^{-1}), t (d) is time, and D_s (m^2 d^{-1}) is the surface diffusion coefficient.

Key limiting factors of algal growth are light, CO_2, N, and P (Lee and Zhang, 2016). Recently, Lee and Zhang (2016) showed that, for NH_4^+-N concentrations ≤ 150 mg L^{-1}, a co-limitation model without inhibition provided a reasonable growth prediction in comparison to experimental *Chlorella* growth data. Therefore, we adopted a Monod expression for the N utilization rate. Light and temperature factors were expressed using the Chalker model combined with the Arrhenius equation, which leads to the following rate equation:

$$r_A = \frac{\mu_{max} C_{NH_4^+} X_A}{Y_A\left(K_{S,NH_4^+} + C_{NH_4^+}\right)} * \theta^{(T-20)} \tanh(I_{av}/I_k) \quad (3)$$

where μ_{max} (d^{-1}) is the maximum specific growth rate, X_A (g L^{-1}) is the algal biomass concentration, Y_A is the yield coefficient (dimensionless), K_{S,NH_4^+} (meq L^{-1}) is the half saturation constant, θ (dimensionless) is the Arrhenius growth coefficient, I_k (μmol photon m^{-2} d^{-1}) is the light half saturation coefficient, T is temperature (^{0}C), and I_{av} (μmol photon m^{-2} d^{-1}) is the average irradiance. The average irradiance term, I_{av} (μmol photon m^{-2} d^{-1}), is included to account for light attenuation in the HAPIX reactor, caused by self-shading by algal biomass and is given by:

$$I_{av} = \frac{I_0}{kdX_A}[1 - \exp(-kdX_A)] \quad (4)$$

where I_0 (μmol photon m^{-2} d^{-1}) is the incident light intensity, k (m^2 g^{-1}) is the light attenuation coefficient, and d (m) is the reactor diameter. Assuming the temporal dynamics of the aqueous phase NH_4^+-N concentration is driven by IX and algal biosynthesis, we combined a Fickian surface diffusion flux term (Eq. (1)) and the algae kinetic rate expression (Eq. (3)) to get the following

expression for the aqueous phase NH_4^+-N concentration:

$$\frac{dC_{NH_4^+}}{dt} = -\frac{3M}{RV}D_s\frac{\partial q_{NH_4^+}}{\partial r}\bigg|_{r=R} - \frac{\mu_{max}C_{NH_4^+}X_A}{Y_A\left(K_{S,NH_4^+}+C_{NH_4^+}\right)}*\theta^{(T-20)}\tanh(I_{av}/I_k) \quad (5)$$

where M (g) is the mass of zeolite, R is the radius of a chabazite particle (m), and V is the volume of liquid (L). We assume no algal biomass decay, so that the phototrophic biomass growth rate can be obtained from the rate equation for algal photosynthesis:

$$\frac{dX_A}{dt} = Y_A r_A \quad (6)$$

To complete the mathematical model, initial conditions are required to solve the HAPIX system represented by Eqs (5) and (6). To simulate the experimental conditions, during the 24-h adsorption phase, no NH_4^+ was assumed to initially be present in the zeolite. When algae were added after the IX phase, both IX and NH_4^+ assimilation by algae occurred (HAPIX phase). The end of the adsorption phase provided the starting point for the simulation of the HAPIX phase. The following equations describe the initial conditions used for the solid phase:

$$q_{NH_4^+}(t=0,r) = 0 \quad \text{for the IX phase} \quad (7)$$

$$q_{NH_4^+}(t=0,r) = q_{hpx} \quad \text{for the HAPIX phase} \quad (8)$$

where $q_{NH_4^+}$ (meq g^{-1}) is initialized to have no adsorbed ions during the first 24 h of the experiment, designated as the IX phase, and q_{hpx} (meq g^{-1}) is initial solid phase concentration during the HAPIX phase. The boundary conditions are given by:

$$\frac{\partial q_{NH_4^+}}{\partial r} = 0, r = 0, t > 0 \quad (9)$$

$$q_{NH_4^+}(r=R,t) = \frac{QKC_{NH_4^+}}{C_{Na^+}+KC_{NH_4^+}} \quad (10)$$

where C_{Na^+} (meq L^{-1}) is the aqueous phase concentration of Na^+, and Q (meq g^{-1}) and K (dimensionless) are constants in the IX isotherm related to maximum adsorption capacity and affinity for the exchanger. Eq. (9) imposes a symmetry boundary condition at the center of a chabazite particle and Eq. (10) assumes that at the surface of the zeolite the aqueous and sorbed phase concentrations of NH_4^+ are in equilibrium. The initial conditions for species in the aqueous phase, and algal biomass concentration are given by:

$$\left\{\begin{array}{l} C_{NH_4^+}(t=0) = C_{0,NH_4^+} \\ C_{Na^+}(t=0) = C_{0,Na^+} \\ X_A(t=0) = X_{0,A} \end{array}\right\} \quad (11)$$

where the terms on the right-hand side of Eq. (11) were initialized according to the observed experimental conditions. The model was implemented in Matlab 2016 (MathWorks, US). Details on the numerical implementation of the HAPIX model are discussed in the supplementary information (S2).

4. Results and discussion

4.1. NH_4^+ removal in HAPIX reactors

Cation concentration results from all HAPIX reactors showed that Na^+ was the major cation exchanged with NH_4^+ (Fig. 2). K^+ in the centrate was also adsorbed by the chabazite. Prior studies have shown that the cation affinity sequence for chabazite is $K^+ > NH_4^+ > Na^+ > Ca^{2+} > Mg^{2+}$ (Hedström, 2001). The presence of K^+ will compete with NH_4^+ for IX sites (Wang and Peng, 2010). However, NH_4^+ concentrations (84 meq L^{-1}) in the centrate were eight times higher than K^+ concentrations (10 meq L^{-1}), thus the effect of competition between K^+ and NH_4^+ was negligible during the initial 24 h of the IX process.

Zeolite dosages of 60, 150 and 250 g L^{-1} reduced the NH_4^+-N concentrations from 1180 mg L^{-1} to 184 ± 40, 107 ± 7, and 53 ± 15 mg L^{-1} after adsorption, respectively (Fig. 2). The FA concentration, which was affected by total ammonia nitrogen (TAN = NH_3-N + NH_4^+-N) concentration, pH, and temperature, was calculated according to Eq. (12) (Anthonisen et al., 1976; Kim et al., 2008):

$$NH_3 - N = \frac{TAN \times 10^{pH}}{\exp[(6334)/(273+T)] + 10^{pH}} \quad (12)$$

where, NH_3-N (mg N L^{-1}) is the concentration of FA, TAN (mg L^{-1}) is the concentration of total ammonia nitrogen, and T (°C) is temperature. The FA concentration of centrate used in this study was 65.8 mg L^{-1}, which is much higher than the threshold inhibition level of algae of 28 mg L^{-1} (Källqvist and Svenson, 2003). Addition of zeolite at 60, 150, and 250 g L^{-1} reduced the FA concentrations to 2.5, 0.7 and 1 mg L^{-1}, respectively, below the inhibitory level for algae.

The growth of algae in IA-60, IA-150 and IA-250 reactors during Phase 1 further reduced the aqueous NH_4^+-N concentrations to 47.3 ± 11.9, 10.5 ± 2.8, and 5.5 ± 0.2 mg L^{-1}, respectively. However, NH_4^+-N concentrations in IX controls without algae remained constant at 140 ± 10, 50 ± 10, and 22 ± 6 mg L^{-1} for IX-60, IX-150, and IX 250, respectively (S3 Figure S3). Harvesting algae and recycling the supernatant in Phases 2 and 3 supported continued growth of algae and maintained stable low NH_4^+-N concentrations in the HAPIX reactors. The NH_4^+-N concentrations of IA-60, IA-150 and IA-250 were reduced to 10.1 ± 0.8, 6.5 ± 0.2 and 6.5 ± 1.1 mg L^{-1} at the end of Phase 3. The 60 g L^{-1} zeolite dosage resulted in significantly higher final NH_4^+ -N concentration ($P = 0.003$) than dosages of 150 and 250 g L^{-1}, while final NH_4^+-N concentrations with zeolite dosages of 150 ad 250 g L^{-1} were not significantly different ($P = 1$). NH_4^+ initially adsorbed in the solid phase of the chabazite was desorbed to support the continuous growth of algae. Assuming the N content in the algal biomass is 9.2% (Wang et al., 2015), the N assimilated by algae during the three phases in IA-60, IA-150, and IA-250 were 146, 115 and 109 mg, respectively. However, the NH_4^+-N removed from aqueous phase, which is the difference of NH_4^+-N mass after adsorption and the final effluent at the end of Phase 3, were 87, 48 and 23 mg for IA-60, IA-150 and IA-250, respectively. The NH_4^+ - N assimilated by algae was higher than that removed from aqueous phase, indicating desorption of NH_4^+ from the solid phase supported the growth of algae.

Note that nitrification and denitrification may have played a small role in N removal in the systems. The inoculum used in this study was enriched in algal biomass. In addition, the HAPIX reactors were continuously illuminated, which favors the growth of algae over nitrifiers. Only a small amount of nitrification and denitrification was observed during the first 24 h of adsorption, however, no nitrite or nitrate was detected 2 days after algae addition.

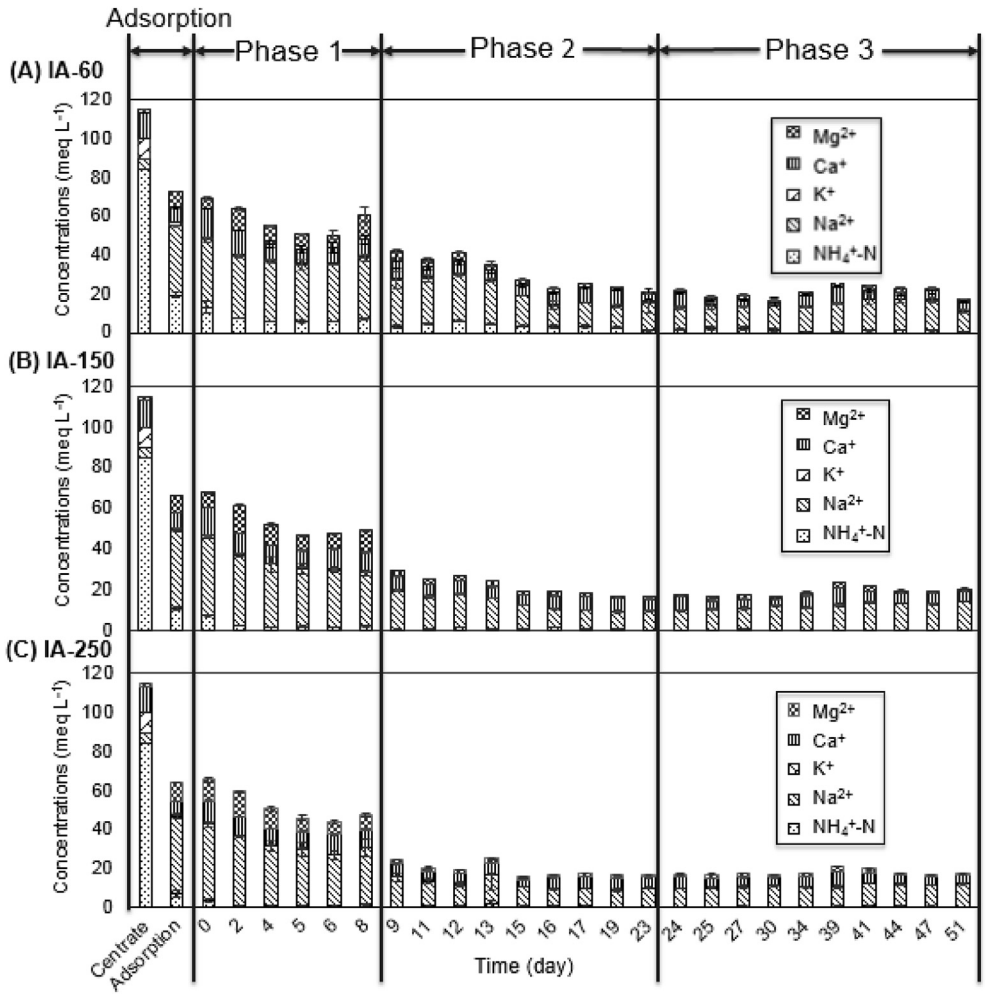

Fig. 2. Temporal changes in cation concentrations in HAPIX reactors (A) IA-60: chabazite dosage of 60 g L^{-1}; (B) IA-150: chabazite dosage of 150 g L^{-1}; and (C) IA-250: chabazite dosage of 250 g L^{-1}. Centrate: cations in the centrate; Adsorption: cations after adsorption for 24 h; Day 0 indicates the time when algae were added; Phase 1: initial algae growth phase; Phase 2 3; algae grown in recycled supernatant.

4.2. Temporal variation of cations in HAPIX reactors

The overall cation concentrations in all the HAPIX reactors showed decreasing trends. Besides IX onto chabazite, several physical, chemical and biological mechanisms may contribute to changes in aqueous phase cation concentrations. The increase in pH from 7.5 to 9.5–10.1 on day 9 likely induced precipitation of Ca^{2+} and Mg^{2+}, which contributed to the decrease in liquid phase cations and conductivity (S4 Figure S4). Similar results were observed by Wang et al. (2016), whereby precipitation contributed to Ca^{2+} and Mg^{2+} removal in an algal system used to treat reverse osmosis concentrate. In addition to chemical precipitation, cell-surface adsorption and intracellular accumulation of metals by algae may have contributed to the decrease in cations (Suresh Kumar et al., 2015). The cell wall of algae consists of polysaccharides, proteins, lipids, and functional groups, such as carboxyl (−COOH), hydroxyl (−OH), phosphate ($-PO_3$), diphosphorus trioxide ($-P_2O_3$), amino ($-NH_2$), sulfhydryl (−SH), amide, primary amine-group, halide-group and aliphatic alkyl-group, which lead to a negative charge of the algal cell surface and a high affinity for cations. Most of the sites bind with Na^+, Ca^{2+} and Mg^{2+} at high pH (González-Dávila, 1995), which may have contributed to the decrease in cations. Furthermore, algae have been shown to favor assimilation of K^+ over Na^+ (Schaedle and Jacobson, 1967). In this study, a slight decrease in Na^+ was observed during Phase 2 after Day 13. The algae biomass most likely started to uptake Na^+ from solution when the K^+ was depleted (Barber and Shieh, 1973).

The presence of anionic complexing ligands or organic matter in the centrate may have also affected the IX capacity of the zeolite. The ligands may compete with the surface for coordination reactions with metal ions (Suresh Kumar et al., 2015). The presence of organic matter may reduce the surface tension of the aqueous phase thereby enhancing the access of ions in the bulk liquid to the pores within the exchanger (Jorgensen and Weatherley, 2003). Further research on cation transport and uptake by algae is needed to identify the mechanisms involved, which will be helpful to understand the fate of cations in HAPIX reactors.

4.3. Algal biomass production

As discussed in Section 4.1, the addition of chabazite decreased the FA concentration below the toxic level for algae at all dosages. Algal biomass in all the HAPIX reactors increased from 500 mg L^{-1} to over 1500 mg L^{-1} by Day 8 prior to harvesting (Fig. 3). However, inhibition of algae growth due to the high NH_4^+ concentrations of the centrate (>1000 mg N L^{-1}) was observed in the algal control reactor without chabazite addition. Algae in IA-60 and IA-150 reached peak biomass concentrations on Day 8. However, algae in

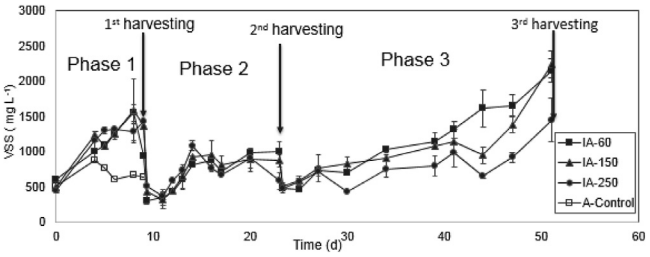

Fig. 3. Algal biomass growth over time. Arrows indicate algae harvesting.

IA-250 reached steady state after only 6 days due to the relatively lower NH_4^+ concentrations in the aqueous phase.

During Phase 3, a longer lag period for the algae growth was observed due to the constant low NH_4^+ concentrations in the aqueous phase. The total algal biomass harvested over the three phases from IA-60, IA-150 and IA-250 were 1587 mg, 1248 mg and 1187 mg, respectively. More algal biomass was harvested from the reactor with lower chabazite dosage. Supernatant was recycled in the reactors during Phases 2 and 3, thus less cations were available for IX with NH_4^+ adsorbed in the solid phase. Introducing fresh centrate with selective cations and creating a concentration gradient between the aqueous and solid phases may increase the selective reversal of NH_4^+ desorption to the aqueous phase. Additionally, the growth of biofilms on the surface of the chabazite during the latter periods of Phases 2 and 3 may have inhibited mass transfer of NH_4^+ from the chabazite to the aqueous phase. A longer lag period is required to stimulate algae growth when less NH_4^+ is available in the aqueous phase.

4.4. Effect of zeolite dosages on intracellular contents of algal biomass

The intercellular contents of algae were regulated by the NH_4^+ concentrations, which could be controlled by modifying chabazite dosages in HAPIX reactors. In this study, protein contents of the harvested algal biomass ranged from 27.7% to 57.1% (by dry weight), and were much higher than starch or lipid contents at all chabazite dosages (Fig. 4). Algae grown in IA-60 had a significantly higher protein content (43.9 and 53.7% for Phase 1 and Phase 3, respectively) in the algal biomass than IA-150 and IA-250. In contrast, differences between protein contents of algae harvested with chabazite dosages of 150 g L^{-1} and 250 g L^{-1} were not significant ($P = 0.73$) due to the similar NH_4^+-N concentration in the liquid phase. The NH_4^+-N concentrations of IA-150 and IA-250 at the end of Phase 1 were 10.5 ± 2.8, and 5.5 ± 0.2 mg L^{-1}, respectively, which were close to that of IA-60 (47.3 ± 11.9 mg L^{-1}). The NH_4^+-N concentration of IA-150 and IA-250 at the end of Phase 3 were 6.5 ± 0.2 and 6.5 ± 1.1 mg L^{-1}, respectively. The differences in the NH_4^+-N concentrations of IA-150 and IA-250 were not high enough to result in significant differences in the protein contents of the algal biomass. Prior studies have shown that proteins in algae are mainly enzymatic proteins, which could be useful as an animal feed source (Becker, 2007).

The starch contents of algal biomass in IA-60, IA-150, and IA-250 during Phase 1 were 6.8, 4.8 and 2.8% by dry weight, respectively. The starch contents of IA-60 and IA-150 in Phase 3 increased to 11.2 and 8.9% by dry weight, respectively. While the starch content of algal biomass in IA-250 was the same as Phase 1, probably due to the increase in ash content of the algal biomass in Phase 3. The VSS to TSS ratio of IA-250 in Phase 3 was only $54 \pm 15\%$. While the VSS to TSS ratio of algal biomass harvested in IA-60 and IA-150 were $80 \pm 8\%$ and $80 \pm 1\%$, respectively. In general, the starch contents decreased with increasing zeolite dosages.

The total lipid as triacylglycerides (TAG) were less than 10% by dry weight for all the chabazite dosages (Fig. 4). Algae harvested in Phase 3 had higher TAG content than Phase 1 at dosages of 60 g L^{-1} (IA-60) and 150 g L^{-1} (IA-150), due to the low aqueous NH_4^+ concentrations in Phase 3. However, the TAG content of IA-250 in Phase 3 was lower than that of Phase 1 because of the high ash content of the algal biomass harvested in Phase 3, as described earlier. Algae grown in wastewater with a high N content tend to have a low lipid content. *C. vulgaris* grown at 247 mg N L^{-1} had lipid content of 5.9% by dry weight (Converti et al., 2009). *Chlorella* grown in centrate from an activated sludge thickening process had a fatty acid methyl ester content of 9.98–11.04% by total VSS (Li et al., 2011). Algae accumulate TAG under N starvation conditions by activate acyltransferase (Shifrin and Chisholm, 1981; Solovchenko et al., 2008; Sukenik and Livne, 1991). For example, *Scenedesmus* sp. accumulated as high as 30% lipid under nitrogen limited conditions (2.5 mg L^{-1}) (Xin et al., 2010a). Deficiency of N from 1.4 mg L^{-1} to 0.31 mg L^{-1} triggered the accumulation of lipid content from 14% to 31% (Xin et al., 2010b). Although the HAPIX reactors significantly reduced the NH_4^+-N concentration of the anaerobically digested centrate to 6.5–10 mg L^{-1} at the end of Phase 3, the N concentration was still not low enough to induce lipid accumulation in the algal biomass. However, using the HAPIX reactors to treat low strength wastewater, such as primary or secondary effluent, may create N deficient conditions that could accumulate high lipid contents in algae for biofuel production.

The lipid content of algae mainly consisted of TAG, which are composed of saturated and unsaturated fatty acids (Wang et al., 2010). Approximately 67–70% of fatty acids in the algal biomass harvested from HAPIX reactors were unsaturated, of which 43%–54% were polyunsaturated fatty acids (Table 2). The fatty acids are

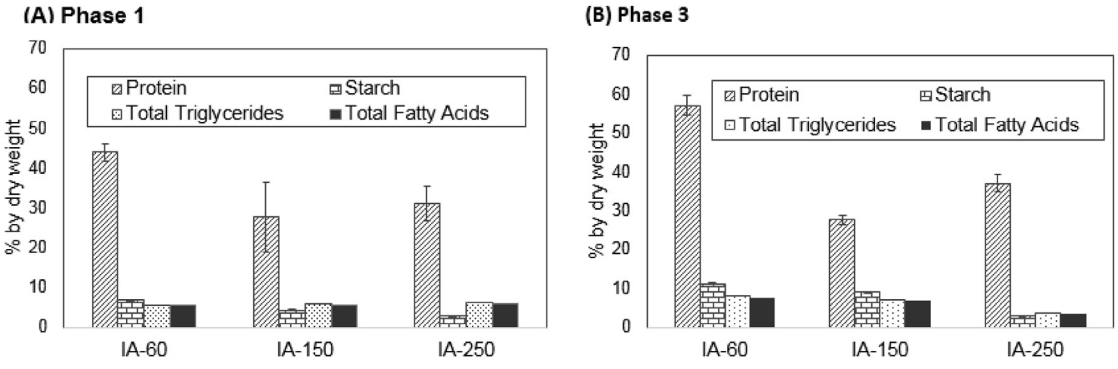

Fig. 4. Intercellular contents of algae harvested in HAPIX reactors.

mainly composed of C16:0, C16:1, C18:0, C18:2 and C18:3, among which palmitic acid (C16:0), oleic acid (C18:1), linoleic acid (C 18:2), and linolenic acid (C 18:3) were the dominant fatty acids. Similar results were found by Wang et al. (2012), where the dominant fatty acids produced by *Chlorella* were hexadecanoic acid (C 16:0), linoleic acid (C 18:2), and linolenic acid (C 18:3). Although the unsaturated fatty acids are an ideal feedstock to produce biofuels, the low fatty acid content in the algae from the HAPIX reactors treating high NH_4^+ strength wastewater (>1000 mg N L^{-1}), make them less economically viable for biofuel production.

4.5. Assessment of mathematical model for HAPIX

4.5.1. HAPIX model parameter determination

Application of the mathematical model requires determination of parameters related to both IX and algal photosynthetic processes. The experimental data for a chabazite dose of 150 g L^{-1} was used for model calibration, while the doses of 60 g L^{-1} and 250 g L^{-1} were used for model validation. Estimation of the parameters for IX was performed in two steps: (i) the maximum ion exchange capacity, *Q*, and the selectivity coefficient, *K*, were fit to batch isotherm data in S1; (ii) the surface diffusion coefficient, D_s, was determined by fitting the HSDM to experimental kinetic data in S1. A limitation of the IX isotherm used in the model is that it considers exchange strictly between NH_4^+ and Na^+. However, a wastewater that contains other background cations, especially K^+, would reduce the rate of uptake of NH_4^+ ions onto chabazite, which would affect the IX capacity, Q, and selectivity coefficient, K, parameters determined in the model. Thus, a future research direction that would enhance the model's applicability in a full-scale system would be to incorporate the effect of K^+ ions on the IX process.

Estimation of the parameters related to algal photosynthesis was done using the following approach: (i) a sensitivity analysis was performed to determine the most sensitive parameters, (ii) the most sensitive parameters were calibrated, whereas the least sensitive parameters were determined from the literature. The sensitivity analysis was conducted using an automated algorithm that uses a Gauss-Newton Levenberg-Marquadt method (Doherty, 2010). The algorithm calculates a dimensionless composite sensitivity value, which is a measure of the impact a change in a parameter value has on model output (Doherty, 2010). Results (Table 3) indicated that the two most sensitive parameters were the light attenuation constant, k (m^2 g^{-1}), and the maximum specific growth rate, μ_{max} (d^{-1}). Calibration of k from 0.2 to 0.8 m^2 g^{-1} and μ_{max} from 0.96 to 0.5 d^{-1} in the developed model led to a good fit of the experimental data. Fig. 5A shows the concentration history of NH_4^+-N in the aqueous phase using the parameters shown in Table 3. The model captures the processes within HAPIX reactor as shown by the removal of most of the NH_4^+ within the first 4 h, followed by a period of relatively constant concentrations.

Fig. 5B shows the experimental data and simulated algal biomass concentration. The model simulation shows an increase in algal biomass concentration corresponding with a decrease in the NH_4^+ -N. The R^2 value of 0.85 suggests that the growth process assuming light and NH_4^+ as limiting factors is sufficient to predict the observed microalgae growth dynamics.

4.5.2. Prediction of NH_4^+ concentrations in aqueous phase

Simulated temporal variations of the NH_4^+-N concentration and experimental data for dosages of 60 and 250 g L^{-1} are shown in Fig. 6. Note that the simulation results only show model correspondence to Phase 1 of the experimental data, since the periodic algal harvesting and recycling of supernatant introduced external factors that may affect the IX process. Thus, it was infeasible to appropriately specify the solid phase NH_4^+ concentrations in Phases 2 and 3, which are required for assigning quantitative initial conditions in the model. The model is in reasonable agreement ($R^2 = 0.83$ and $R^2 = 0.7$) with the observed concentrations, showing that most of the removal occurs within the first 100 h of the HAPIX process. The NH_4^+ removal rates markedly increased with the increase of zeolite dosage within the first 50 h of the HAPIX process because high zeolite dosages have more available IX sites for NH_4^+ adsorption. Overall, for each dosage the model provides a reasonable description of the experimental data. In general, the model predicted lower NH_4^+ concentrations than were observed in the effluent, most likely because mass transfer resistance due to algal biomass growth was neglected. In this study, the chabazite sank to the bottom of the reactors, where limited light was available for the algal biofilm growth on the surface of the chabazite. However, there is more surface area of the highest chabazite dosage (250 g L^{-1}) for algal biofilm growth. Incorporating mass transfer resistance caused by the presence of a biofilm on the zeolite surface would reduce the rate at which ions diffuse into the zeolite, which would lead to an improved representation of the data. However, a caveat is that an additional parameter, a mass transfer coefficient, would need to be introduced, which would require further experimental justification.

Model and experimental microalgae growth results for Phase 1 of HAPIX operation for dosages of 60 and 250 g L^{-1} are shown in Fig. 7A and B. The model prediction is in good agreement ($R^2 = 0.98$) with the experimental data for a dose of 60 g L^{-1}. However, for a dose 250 g L^{-1} the model does not predict as rapid a rate of biomass growth observed experimentally ($R^2 = 0.58$). This slower growth rate predicted by the model is most likely because

Table 2
Profiles of fatty acids of algae harvested in HAPIX reactors from Phase 1 and Phase 3 (% of total fatty acids).

Parameters	Samples					
	Phase 1			Phase 3		
	IA-60	IA-150	IA-250	IA-60	IA-150	IA-250
C16:0 (Palmitic Acid)	23%	23%	23%	26%	25%	24%
C16:1 Total (Palmitoleic Acid + isomers)	6%	5%	5%	4%	5%	5%
C 16:4 (Hexadecatetraenoic Acid)	2%	2%	1%	0%	0%	0%
C18:0 (Stearic Acid)	1%	2%	1%	1%	1%	1%
C18:1, Total (Oleic Acid + isomers)	19%	22%	19%	11%	12%	13%
C18:2, Total (Linoleic Acid + isomers)	28%	28%	30%	47%	45%	41%
C18:3, Total (Linolenic Acid + isomers)	18%	14%	16%	8%	10%	12%
Other Fatty Acids	3%	4%	5%	3%	2%	4%
Total Monounsaturated Fatty Acids	21%	24%	22%	15%	16%	17%
Total Polyunsaturated Fatty Acids	46%	43%	46%	54%	54%	53%
Total Saturated Fatty Acids	27%	28%	26%	30%	29%	29%
Total Trans Fatty Acid	6%	6%	5%	1%	1%	1%

Table 3
Parameters used in numerical simulation of concentration profiles and the sensitivity scores.

Parameter	Definition	Value	Source	Sensitivity score
IX Model Parameters				
K	Selectivity coefficient	2.9 (dimensionless)	Calibrated to isotherm data (S1)	Not calculated
Q	Maximum ion exchange capacity	2.8 meq g^{-1}	Calibrated to isotherm data (S1)	Not calculated
D_s	Surface diffusion coefficient	$9.1x10^{-12}$ m^2 d^{-1}	Calibrated to kinetic data (S1)	Not calculated
Algal Photosynthesis Parameters				
K_{S,NH_4^+}	Half saturation coefficient	0.36 meq L^{-1}	Lee and Zhang, 2016	0.000001
μ_{max}	maximum algae growth rate	0.5 d^{-1}	Calibrated	73.7
k	Light attenuation rate	0.8 m^2 g^{-1}	Calibrated	24.1
θ	Arrhenius growth coefficient	1.35 (dimensionless)	Lee and Zhang, 2016	16.8
I_0	Incident light intensity	100 μmol photon s^{-1}	Measured	
I_k	Light saturation point	16.9 μmol photon s^{-1}	Lee and Zhang, 2016	0.00168

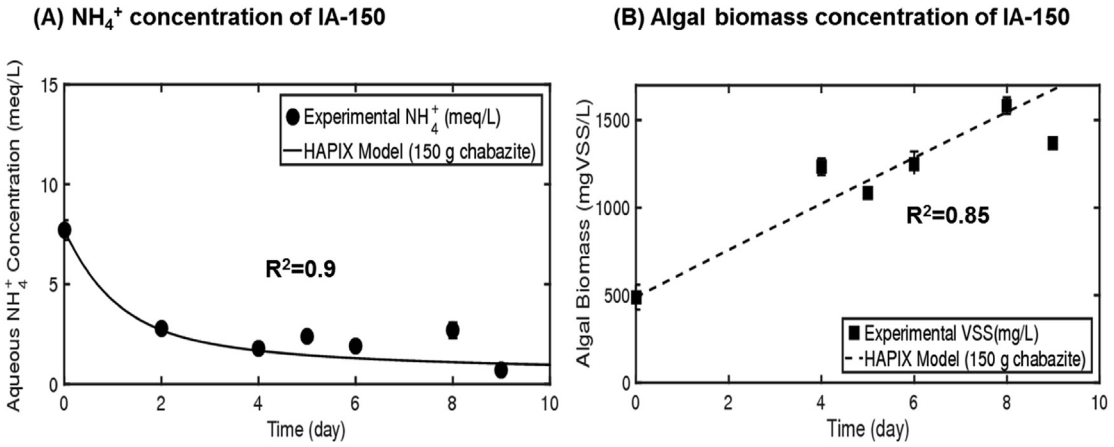

Fig. 5. (A) NH_4^+ concentration in HAPIX reactor over time; (B) Algal biomass concentration in HAPIX reactor over time. Chabazite dosage of 150 g L^{-1}.

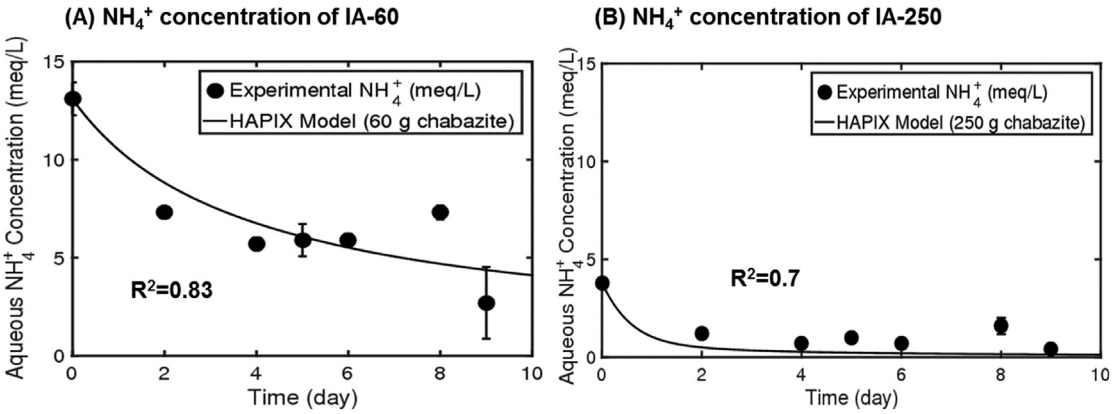

Fig. 6. NH_4^+ concentration history in HAPIX reactor over time (A) dosage of 60 g L^{-1}, (B) dosage of 250 g L^{-1}.

the highest dosage resulted in lowest aqueous phase NH_4^+ concentrations, so less N was available to support algal growth. Nevertheless, the model captures the trend of the algae growth data, showing linear growth characteristics. This positive trend corresponds with the utilization of NH_4^+-N in solution and conversion of light, nutrients and CO_2 to new algal cells. The model behavior is consistent with recent findings from the model developed by Lee and Zhang, (2016), which was fit to experimental algal biomass growth for centrate of various characteristics.

5. Conclusions

This research demonstrated that the HAPIX process is suitable for treatment of high NH_4^+ strength wastewater (>1000 mg N L^{-1}) without dilution. Zeolite dosages of 60, 150 and 250 g L^{-1} resulted in stable NH_4^+-N concentrations, lower than 10.1 ± 0.8 mg L^{-1} in the effluent. Algae control reactors without zeolite addition showed no algae growth. The IX process reduced the FA of the centrate from 4.7 mM to <0.18 mM, and promoted algae growth. Different

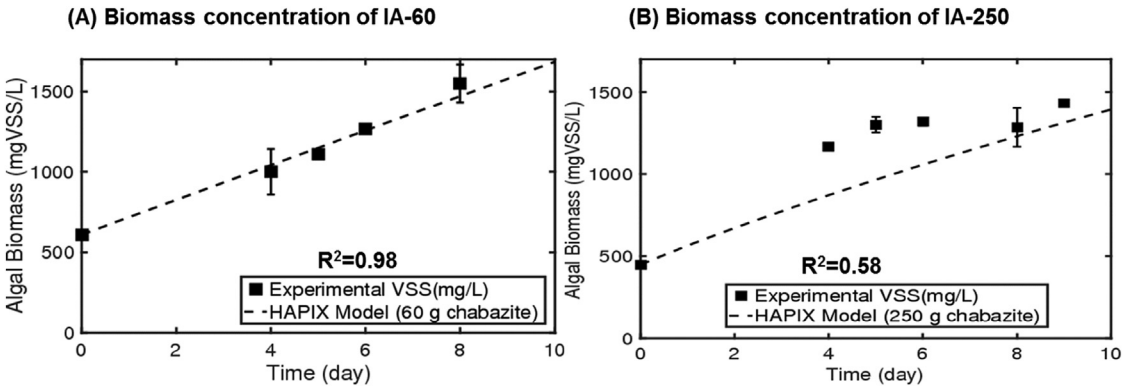

Fig. 7. Algae biomass concentration in HAPIX reactors over time, (A) dosage of 60 g L^{-1}, (B) dosage of 250 g L^{-1}.

dosages of zeolite resulted in different NH_4^+-N concentrations in the aqueous phase and different protein and starch contents of the algal biomass. Zeolite dosages at 60 g L^{-1} resulted in higher protein and starch contents in the algal biomass than doses of 150 g L^{-1} and 250 g L^{-1}. Valuable products may be extracted from the harvested algal biomass due to the high protein content (27%–57% by dry weight). About 67–70% of the fatty acid in the algal biomass were unsaturated fatty acids. The lipid contents in all the cultures were lower than 10%, which are not economically feasible to produce biofuels. A mathematical model describing the HAPIX process was developed that predicts the fate of NH_4^+-N and algal biomass growth over time. The light attenuation constant (k) and the maximum specific growth rate (μ_{max}) were the most sensitive parameters in the model. Calibration of k from 0.2 to 0.8 m^2 g-1 and μ_{max} from 0.96 to 0.5 d^{-1} in the developed model led to a good fit of the experimental data. The HAPIX process serves a two-fold purpose: treatment of high NH_4^+-N strength wastewater and production of agricultural and commercial biopolymers. The main limitation of the modeling framework is that the model does not account for algal biomass growth on the zeolite with time. Future work could be focused on accounting for both suspended and attached growth into the model. Moreover, the model can be integrated with computational fluid dynamics models to simulate the performance of the HAPIX process for a full-scale system.

Acknowledgements

This material is based upon work supported by the National Science Foundation under Grant Nos. 1243510 and 1511439. Any opinions, findings, and conclusions or recommendations expressed in this material are those of the authors and do not necessarily reflect the views of the National Science Foundation. We would like to thank Dr. Jie Zhang at Carollo Engineers who provided valuable suggestions on this paper. We also thank the anonymous reviewers' comments to improve the quality of this manuscript.

Appendix A. Supplementary data

Supplementary data related to this article can be found at https://doi.org/10.1016/j.watres.2018.05.043.

References

Amini, A., Aponte-Morales, V., Wang, M., Dilbeck, M., Lahav, O., Zhang, Q., Cunningham, J.A., Ergas, S.J., 2017. Cost-effective treatment of swine wastes through recovery of energy and nutrients. Waste Manag. 69 (Suppl. C), 508–517.

Anthonisen, A.C., Loehr, R.C., Prakasam, T.B.S., Srinath, E.G., 1976. Inhibition of nitrification by ammonia and nitrous acid. J. Water Pollut. Control Fed. 48 (5), 835–852.

APHA, AWWA, WEF, 2012. Standard Methods for the Examination of Water and Wastewater. American Public Health Association, Washington, D. C.

Aponte-Morales, V.E., 2015. Ammonium Removal from High Strength Wastewater Using a Hybrid Ion Exchange Biological Process.

Aponte-Morales, V.E., Tong, S., Ergas, S.J., 2016. Nitrogen removal from anaerobically digested swine waste centrate using a laboratory-scale chabazite-sequencing batch reactor. Environ. Eng. Sci. 33 (5), 324–332.

Aponte-Morales, V.E., Payne, K.A., Cunningham, J.A., Ergas, S.J., 2018. Bio-regeneration of chabazite during nitrification of centrate from anaerobically digested biosolids: experimental and modeling studies. Environ. Sci. Technol. 52 (7), 4090–4098.

Auerbach, S.M., Carrado, K.A., Dutta, P.K., 2003. Handbook of Zeolite Science and Technology. CRC press.

Barber, J., Shieh, Y.J., 1973. Sodium transport in Na+-rich Chlorella cells. Planta 111 (1), 13–22.

Becker, E.W., 2007. Micro-algae as a source of protein. Biotechnol. Adv. 25 (2), 207–210.

Cantrell, K.B., Ducey, T., Ro, K.S., Hunt, P.G., 2008. Livestock waste-to-bioenergy generation opportunities. Bioresour. Technol. 99 (17), 7941–7953.

Converti, A., Casazza, A.A., Ortiz, E.Y., Perego, P., Del Borghi, M., 2009. Effect of temperature and nitrogen concentration on the growth and lipid content of Nannochloropsis oculata and Chlorella vulgaris for biodiesel production. Chem. Eng. Process: Process Intensification 48 (6), 1146–1151.

Crofts, A.R., 1966. Uptake of ammonium ion by chloroplasts, and its relation to photophosphorylation. Biochem. Biophys. Res. Commun. 24 (5), 725–731.

Doherty, J., 2010. PEST Model-independent parameter estimation, 5th ed. Watermark Numerical Computing, Brisbane, Australia.

Fux, C., Velten, S., Carozzi, V., Solley, D., Keller, J., 2006. Efficient and stable nitritation and denitritation of ammonium-rich sludge dewatering liquor using an SBR with continuous loading. Water Res. 40 (14), 2765–2775.

González-Dávila, M., 1995. The role of phytoplankton cells on the control of heavy metal concentration in seawater. Mar. Chem. 48 (3), 215–236.

Halfhide, T., Dalrymple, O., Wilkie, A., Trimmer, J., Gillie, B., Udom, I., Zhang, Q., Ergas, S., 2014. Growth of an indigenous algal consortium on anaerobically digested municipal sludge centrate: photobioreactor performance and modeling. BioEnergy Res. 1–10.

Hedström, A., 2001. Ion exchange of ammonium in zeolites: a literature review. J. Environ. Eng. 127 (8), 673–681.

Jorgensen, T.C., Weatherley, L.R., 2003. Ammonia removal from wastewater by ion exchange in the presence of organic contaminants. Water Res. 37 (8), 1723–1728.

Juneja, A., Ceballos, R., Murthy, G., 2013. Effects of environmental factors and nutrient availability on the biochemical composition of algae for biofuels production: a review. Energies 6 (9), 4607.

Källqvist, T., Svenson, A., 2003. Assessment of ammonia toxicity in tests with the microalga, Nephroselmis pyriformis, Chlorophyta. Water Res. 37 (3), 477–484.

Kim, Y.M., Park, D., Lee, D.S., Park, J.M., 2008. Inhibitory effects of toxic compounds on nitrification process for cokes wastewater treatment. J. Hazard Mater. 152 (3), 915–921.

Kjeldsen, P., Barlaz, M.A., Rooker, A.P., Baun, A., Ledin, A., Christensen, T.H., 2002. Present and long-term composition of MSW landfill leachate: a review. Crit. Rev. Environ. Sci. Technol. 32 (4), 297–336.

Kotay, S.M., Mansell, B.L., Hogsett, M., Pei, H., Goel, R., 2013. Anaerobic ammonia oxidation (ANAMMOX) for side-stream treatment of anaerobic digester filtrate process performance and microbiology. Biotechnol. Bioeng. 110 (4), 1180–1192.

Krishna, R., Wesselingh, J.A., 1997. The Maxwell-Stefan approach to mass transfer. Chem. Eng. Sci. 52 (6), 861–911.

Lackner, S., Gilbert, E.M., Vlaeminck, S.E., Joss, A., Horn, H., van Loosdrecht, M.C.M., 2014. Full-scale partial nitritation/anammox experiences – an application survey. Water Res. 55 (Suppl. C), 292–303.

Lee, E., Zhang, Q., 2016. Integrated co-limitation kinetic model for microalgae

growth in anaerobically digested municipal sludge centrate. Algal Res. 18, 15–24.
Li, Y., Chen, Y.-F., Chen, P., Min, M., Zhou, W., Martinez, B., Zhu, J., Ruan, R., 2011. Characterization of a microalga Chlorella sp. well adapted to highly concentrated municipal wastewater for nutrient removal and biodiesel production. Bioresour. Technol. 102 (8), 5138–5144.
Lin, L., Chan, G.Y.S., Jiang, B.L., Lan, C.Y., 2007. Use of ammoniacal nitrogen tolerant microalgae in landfill leachate treatment. Waste Manag. 27 (10), 1376–1382.
Lito, P.F., Aniceto, J.P.S., Silva, C.M., 2014. Modelling ion exchange kinetics in zeolyte-type materials using Maxwell-Stefan approach. Desalination Water Treat. 52 (28–30), 5333–5342.
Malovanyy, A., Sakalova, H., Yatchyshyn, Y., Plaza, E., Malovanyy, M., 2013. Concentration of ammonium from municipal wastewater using ion exchange process. Desalination 329 (0), 93–102.
Martins, T.H., Souza, T.S.O., Foresti, E., 2017. Ammonium removal from landfill leachate by Clinoptilolite adsorption followed by bioregeneration. J. Environ. Chem. Eng. 5 (1), 63–68.
Park, J., Jin, H.-F., Lim, B.-R., Park, K.-Y., Lee, K., 2010. Ammonia removal from anaerobic digestion effluent of livestock waste using green alga Scenedesmus sp. Bioresour. Technol. 101 (22), 8649–8657.
Rožić, M., Cerjan-Stefanović, Š., Kurajica, S., Vančina, V., Hodžić, E., 2000. Ammoniacal nitrogen removal from water by treatment with clays and zeolites. Water Res. 34 (14), 3675–3681.
Rusten, B., Sahu, A.K., 2011. Microalgae growth for nutrient recovery from sludge liquor and production of renewable bioenergy. Water Sci. Technol. 64 (6), 1195–1201.
Schaedle, M., Jacobson, L., 1967. Ion absorption and retention by Chlorella pyrenoidosa. III. Selective accumulation of rubidium, potassium and sodium. Plant Physiol. 42 (7), 953–958.
Shifrin, N.S., Chisholm, S.W., 1981. Phytoplankton lipids: interspecific differences and effects of nitrate, silicate and light-dark cycles. J. Phycol. 17 (4), 374–384.
Solovchenko, A.E., Khozin-Goldberg, I., Didi-Cohen, S., Cohen, Z., Merzlyak, M.N., 2008. Effects of light intensity and nitrogen starvation on growth, total fatty acids and arachidonic acid in the green microalga Parietochloris incisa. J. Appl. Phycol. 20 (3), 245–251.
Sukenik, A., Livne, A., 1991. Variations in lipid and fatty acid content in relation to acetyl CoA carboxylase in the marine prymnesiophyte Isochrysis galbana. Plant Cell Physiol. 32 (3), 371–378.
Suresh Kumar, K., Dahms, H.-U., Won, E.-J., Lee, J.-S., Shin, K.-H., 2015. Microalgae – a promising tool for heavy metal remediation. Ecotoxicol. Environ. Saf. 113 (Suppl. C), 329–352.
Tada, C., Yang, Y., Hanaoka, T., Sonoda, A., Ooi, K., Sawayama, S., 2005. Effect of natural zeolite on methane production for anaerobic digestion of ammonium rich organic sludge. Bioresour. Technol. 96 (4), 459–464.
Tarpeh, W.A., Udert, K.M., Nelson, K.L., 2017. Comparing ion exchange adsorbents for nitrogen recovery from source-separated urine. Environ. Sci. Technol. 51 (4), 2373–2381.
Third, K.A., Paxman, J., Schmid, M., Strous, M., Jetten, M.S.M., Cord-Ruwisch, R., 2005. Treatment of nitrogen-rich wastewater using partial nitrification and Anammox in the CANON process. Water Sci. Technol. 52 (4), 47–54.
Udert, K.M., Fux, C., Münster, M., Larsen, T.A., Siegrist, H., Gujer, W., 2003. Nitrification and autotrophic denitrification of source-separated urine. Water Sci. Technol. 48 (1), 119–130.
Wang, H., Xiong, H., Hui, Z., Zeng, X., 2012. Mixotrophic cultivation of Chlorella pyrenoidosa with diluted primary piggery wastewater to produce lipids. Bioresour. Technol. 104 (Suppl. C), 215–220.
Wang, L., Li, Y., Chen, P., Min, M., Chen, Y., Zhu, J., Ruan, R.R., 2010. Anaerobic digested dairy manure as a nutrient supplement for cultivation of oil-rich green microalgae Chlorella sp. Bioresour. Technol. 101 (8), 2623–2628.
Wang, M., Park, C., 2015. Investigation of anaerobic digestion of Chlorella sp. and Micractinium sp. grown in high-nitrogen wastewater and their co-digestion with waste activated sludge. Biomass Bioenergy 80, 30–37.
Wang, M., Yang, H., Ergas, S.J., van der Steen, P., 2015. A novel shortcut nitrogen removal process using an algal-bacterial consortium in a photo-sequencing batch reactor (PSBR). Water Res. 87, 38–48.
Wang, S., Peng, Y., 2010. Natural zeolites as effective adsorbents in water and wastewater treatment. Chem. Eng. J. 156 (1), 11–24.
Wang, X.-X., Wu, Y.-H., Zhang, T.-Y., Xu, X.-Q., Dao, G.-H., Hu, H.-Y., 2016. Simultaneous nitrogen, phosphorous, and hardness removal from reverse osmosis concentrate by microalgae cultivation. Water Res. 94 (Suppl. C), 215–224.
Wett, B., Alex, J., 2003. Impacts of separate rejection water treatment on the overall plant performance. Water Sci. Technol. 48 (4), 139–146.
Xin, L., Hong-ying, H., Ke, G., Ying-xue, S., 2010a. Effects of different nitrogen and phosphorus concentrations on the growth, nutrient uptake, and lipid accumulation of a freshwater microalga Scenedesmus sp. Bioresour. Technol. 101 (14), 5494–5500.
Xin, L., Hong-Ying, H., Jia, Y., 2010b. Lipid accumulation and nutrient removal properties of a newly isolated freshwater microalga, *Scenedesmus* sp. LX1, growing in secondary effluent. New Biotechnol. 27 (1), 59–63.
Yuan, X., Wang, M., Park, C., Sahu, A.K., Ergas, S.J., 2012. Microalgae growth using high-strength wastewater followed by anaerobic Co-digestion. Water Environ. Res. 84 (5), 396–404.